Computation of the Mid-Sagittal Plane in 3D Images of the Brain

Sylvain Prima, Sébastien Ourselin, and Nicholas Ayache

INRIA Sophia Antipolis, EPIDAURE Project,
2004, route des Lucioles, BP 93,
06902, Sophia Antipolis Cedex, France
{sprima,sourseli,na}@sophia.inria.fr

Abstract. We present a new symmetry-based method allowing to automatically compute, reorient and recenter the mid-sagittal plane in anatomical and functional 3D images of the brain. Our approach is composed of two steps. At first, the computation of local similarity measures between the two hemispheres of the brain allows to match homologous anatomical structures or functional areas, by way of a block matching procedure. The output is a set of point-to-point correspondences: the centers of homologous blocks. Subsequently, we define the mid-sagittal plane as the one best superposing the points in one side of the brain and their counterparts in the other side by reflective symmetry. The estimation of the parameters characterizing the plane is performed by a least trimmed squares optimization scheme. This robust technique allows normal or abnormal asymmetrical areas to be treated as outliers, and the plane to be mainly computed from the underlying gross symmetry of the brain. We show on a large database of synthetic images that we can obtain a subvoxel accuracy in a CPU time of about 3 minutes, for strongly tilted heads, noisy and biased images. We present results on anatomical (MR, CT), and functional (SPECT and PET) images.

1 Introduction

1.1 Presentation of the Problem

A normal human head exhibits a rough bilateral symmetry. What is easily observable for external structures (ears, eyes, nose...) remains valuable for the brain and its components. It is split into two hemispheres, in which each substructure has a counterpart of approximately the same shape and location in the opposite side (frontal, occipital lobes, ventricles...). They are connected to each other by the corpus callosum, and separated by a grossly planar, mid-sagittal, fissure.

However, it has been reported since the late 19th century that conspicuous morphological differences between the hemispheres make the brain systematically asymmetrical. For example, the wider right frontal and left occipital lobes give rise to a torque effect of the overall brain shape (see Fig. 1). More subtly, the natural variability of the cortex translates into slight differences between hemispheres. In the same way, cerebral dominance has been demonstrated since

D. Vernon (Ed.): ECCV 2000, LNCS 1843, pp. 685–701, 2000.

the work of Paul Broca on the language lateralization (1861), and many brain functions are now thought or known to be located in mainly one of the hemispheres (handedness, visual abilities, *etc.*). The question of whether the anatomical and the functional brain asymmetries relate to each other remains debatable to the point, even if evidences of close connections have been demonstrated quite lately [5]. These studies suggest that symmetry considerations are key to the understanding of cerebral functioning.

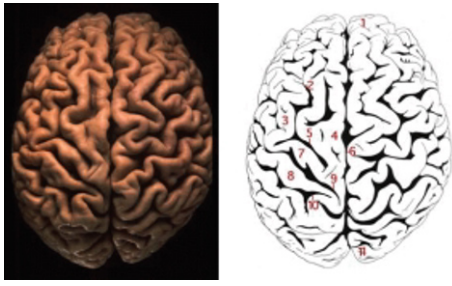

Fig. 1. Torque effect of the brain. The right frontal lobe (1) is larger than the left one, and this is the opposite for the occipital lobe (11). Description of the hemispheres: 1. Frontal pole 2. Superior frontal sulcus 3. Middle frontal gyrus 4. Superior frontal gyrus 5. Precentral sulcus 6. Longitudinal cerebral fissure 7. Precentral gyrus 8. Postcentral gyrus 9. Central sulcus 10. Postcentral sulcus 11. Occipital pole. This illustration comes from the Virtual Hospital [22].

Volumetric medical images convey information about anatomical (MR, CT) or functional (PET, SPECT) symmetries and asymmetries, but they are hidden by the usual tilt of the patient's head in the device during the scanning process. More precisely, the "ideal" coordinate system attached to the head, in which the inter-hemispheric fissure is conveniently displayed, differs from the coordinate system of the image by three angles around the bottom-top (yaw angle, axial rotation), the back-front (roll angle, coronal rotation) and the left-right (pitch angle, sagittal rotation) axes, and three translations along these directions (see Fig. 2). It means that the fissure is generally not displayed in the center of the image lattice. This prevents from further visual inspection or analysis, because the homologous anatomical structures or functional areas in both hemispheres are not displayed in the same axial or coronal slice in the 3D image.

It is of great interest to correctly reorient and recenter brain images, because normal (torque effect, intrinsic variability) and abnormal (unilateral pathologies) departures from symmetry appear more clearly and make the diagnosis easier in many cases: fractures of the skull in CT images, lesions, or bleed in MR images, asymmetries of perfusion in SPECT images, *etc.* Some diseases are assumed to be strongly linked with abnormalities of brain asymmetry, like schizophrenia: in this case, the brain is suspected to be more symmetrical than normal [4]. After the initial tilt has been corrected, it is easier to perform further manual or automatic measurements to compare the two sides of the brain, because relative locations of homologous structures become immediate to assess [6,12,19].

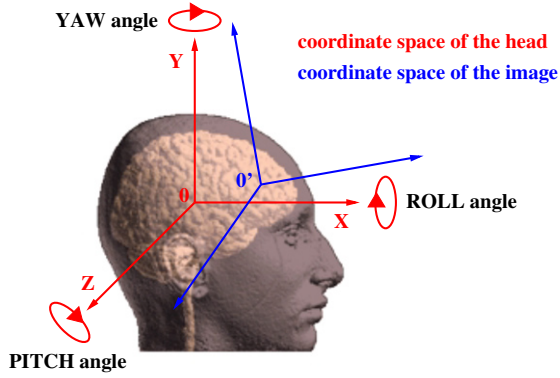

Fig. 2. The "ideal" coordinate system attached to the head (in which the fissure is close to the plane $Z = 0$) and the coordinate system of the image are deduced to each other by way of three angles (yaw, roll and pitch) and a 3D translation ($\overrightarrow{OO'}$).

Several papers have previously considered the problem of correcting the axial and coronal rotations, and the translation along the left-right axis; we give a brief overview of the state-of-the-art in the next section. We do not tackle the problem of correcting the sagittal rotation (e.g., alignment along the AC-PC line) and the translations along the bottom-top and the back-front axes.

1.2 Existing Methods

Most of the existing algorithms share a common methodology. First, a suitable mid-sagittal plane is defined in the brain. Then, this latter is rotated and centered, so that the estimated plane matches the center of the image lattice. There are mainly two classes of methods, differing in their definition of the searched plane. We briefly describe their advantages and drawbacks in the following.

Methods based on the inter-hemispheric fissure The basic hypotheses underlying these methods are that the inter-hemispheric fissure is roughly planar, and that it provides a good landmark for further volumetric symmetry analysis. Generally, the fissure is segmented in MR images, using snakes [6], or a Hough transform [3], and the plane best fitting the segmentation is estimated. As this approach focuses on the inter-hemispheric fissure, the resulting reorientation and recentering of the brain is insensitive to strong asymmetries. Conversely, as the global symmetry of the whole brain is not considered, the resulting algorithms are very sensitive to the often observed curvature of the fissure, which can lead to a meaningless plane (see Fig. 1). At last, these methods are not adaptable to other modalities, where the fissure is not clearly visible.

Methods based on a symmetry criterion There are relatively simple methods of finding a plane of reflective symmetry in case of perfectly symmetrical geometrical objects, in 2D or 3D. In this case, it can be demonstrated that any symmetry plane of a body is perpendicular to a principal axis. In case of medical

images, the problem is different, because normal and abnormal asymmetries deviate the underlying symmetry of the brain: a perfect symmetry plane does not exist. To tackle this problem, an intuitive idea is to define the mid-sagittal plane as the one that maximizes the similarity between the image and its symmetric, i.e., the plane with respect to which the brain exhibits maximum symmetry. Practically, this approximate symmetry plane is to be close to the fissure, but is computed using the whole 3D image and no anatomical landmarks.

Most often, the chosen similarity criterion is the cross correlation, computed between either the intensities [1,7,8] or other features of the two symmetrical images with respect to a plane with given parameters. For example, the criterion can be computed between the derived Extended Gaussian Image (EGI) and its flipped version [17]: theoretically, if the brain is symmetrical, so is its EGI. Contrary to the first class of methods, the whole 3D volume is taken into account, which means that the overall gross symmetry of the brain is used. Consequently, these methods are less sensitive to the variability of the inter-hemispheric fissure and its curved shape. The trade-off is the need for the criterion to be robust with respect to departures from the gross underlying cerebral symmetry, i.e., the normal and pathological asymmetries of the brain. This robustness is difficult to achieve with global criteria such as the cross correlation, that is affected in the same way by areas in strong (i.e., symmetrical) and weak (i.e., asymmetrical) correlation. These latter can severely bias the estimation of the plane [1]. To overcome this issue, another similarity criterion is proposed in [10]: the stochastic sign change, previously shown to be efficient in case of rigid registration, even for quite dissimilar images [20]. In the same way, a specific symmetry measure introduced in [16] considers mainly strongly symmetrical parts of the brain.

One common drawback of these methods is the computational cost of the algorithms, due to the optimization scheme within the set of possible planes. However, this cost can be often reduced: the discretization of the parameters space (that limits the accuracy of the results) or a prior knowledge about the position of the optimal plane allow to investigate only a limited number of planes. Thus, the reorientation of the principal axes of the brain and the centering of its center of mass is often a useful preprocessing step. A multi-resolution scheme can also accelerate the process [1]. One important feature of these approaches is their ability to tackle other modalities than MR, in particular functional images.

1.3 Overview of the Paper

In this article, we present a new symmetry-based method allowing to compute, reorient and recenter the mid-sagittal plane in anatomical and functional images of the brain. This method, generalizing an approach we previously described in [12,19], is composed of two steps. At first, the computation of local rather than global similarity measures between the two sides of the brain allows to match homologous anatomical structures or functional areas, by way of a block matching procedure. The output is a set of point-to-point correspondences: the centers of homologous blocks. Subsequently, we define the mid-sagittal plane as the one best superposing the points in one hemisphere and their counterparts in

the other hemisphere by reflective symmetry. The estimation of the parameters characterizing the plane is performed by a least trimmed squares optimization scheme. Then, the estimated plane is aligned with the center of the image lattice. This method is fully automated, objective and reproducible.

This approach deals with two severe drawbacks of classical symmetry-based methods. First, the computation of local measures of symmetry and the use of a robust estimation technique [15] allow to discriminate between symmetrical and asymmetrical parts of the brain, these latter being naturally treated as outliers. Consequently, the computation of the mid-sagittal plane mainly relies on the underlying gross symmetry of the brain. Second, the regression step yields an analytical solution, computationally less expensive than the maximization of the global similarity measures described in Section 1.2.

We describe this approach in Section 2. In Section 3, we show that we can cope with strongly asymmetrical and tilted brains, even in presence of noise and bias, with very good accuracy and low computation time. In Section 4, we present results on anatomical (MR, CT) and functional (PET, SPECT) images.

2 Description of the Method

2.1 Presentation of the Main Principles

We recall the principles of the method presented in [12,19]. Given I, an MR image of the head, the mid-sagittal plane P is defined as the one best superposing the pairs $\{a_i, S_P(b_i)\}$, where a_i is a brain voxel, b_i its anatomical counterpart in the other hemisphere, and S_P the symmetry with respect to P. Practically, P is obtained by minimization of the least squares (LS) criterion $\sum_i ||a_i - S_P(b_i)||^2$; $||.||$ is the Euclidian norm. An analytical solution of this problem is described in the appendix. The pairs $\{a_i, b_i\}$ are obtained as follows (see also Fig. 3):

- The mid-sagittal plane K of the image grid (K is fixed to the grid) differs from the searched mid-sagittal plane P of the brain in the tilt of the head during the scanning process, but is usually a good first estimate. The original image I is flipped with respect to K, yielding $S_K(I)$.
- The "demons" algorithm [18] finds the anatomical counterpart b'_i in $S_K(I)$ of each point a_i in I, by way of non-rigid registration between the 2 images.
- $b_i = S_K(b'_i)$ is the anatomical counterpart of a_i in the other hemisphere. For example, in I, the point a_i, located at the top of the right ventricle is matched with the point b_i, located at the top of the left ventricle.

Once P is computed, the transformation $R = S_K \circ S_P$ is a rotation if P and K are not parallel and a translation if P and K are parallel. The transformation $R^{1/2}$, when applied to the image I, automatically aligns the plane P with K [19]. Several difficulties and limitations arise when using this method:

- As many of the classical symmetry-based methods, normal and pathological asymmetries can severely disrupt the computation of the plane. Even

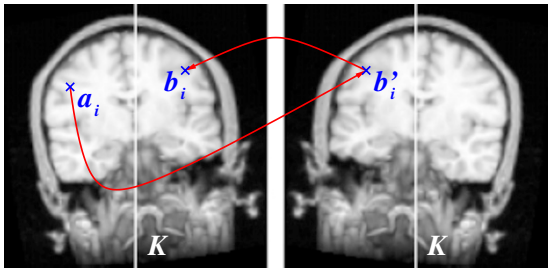

Fig. 3. The non-rigid registration strategy. The point b'_i in $S_K(I)$ is matched with the point a_i in I; $b_i = S_K(b'_i)$ is the counterpart of a_i in the other hemisphere.

though it is based on local instead of global measures of symmetry, the LS minimization is not robust with respect to outliers [15], and will be strongly affected by the departures from the underlying symmetry.
- The non-rigid registration algorithm will provide aberrant matchings when a structure is absent in one hemisphere (a lesion, one track of white matter, *etc.*), or when two structures are present but too different from each other; these failures are difficult if not impossible to detect. These meaningless correspondences can significantly affect the LS criterion and its minimization.
- At last, the "demons" algorithm mainly relies on the gradient of the image, and proved to be efficient for low-textured images like MR or CT. Consequently, this approach is not applicable to SPECT or PET images.

2.2 Modification Based on a Block Matching Strategy and a Robust Estimation Technique

We propose a modification of this approach, allowing to compute the mid-sagittal plane mainly from correspondences between very symmetrical areas, and to tackle both functional and anatomical images. The methodology is twofold: we still find point-to-point correspondences between the two sides of the brain, and then derive the plane best superposing the pairs of matched points, but the matching and the optimization procedures significantly differ from Section 2.1.

Computation of inter-hemispheric correspondences by a block matching strategy. The pairs of correspondences $\{a_i, b'_i\}$ are obtained by way of a block matching strategy between the image I and its symmetric $S_K(I)$. This procedure is extensively described in [11], in case of rigid registration of anatomical sections. The common lattice of the 2 images (of size $X \times Y \times Z$) defines a set of rectangular parallelepipedic blocks of voxels $\{\mathrm{B}\}$ in I and $\{\mathrm{B}'\}$ in $S_K(I)$, given their size $N_x \times N_y \times N_z$: both images contain $(X - N_x + 1) \times (Y - N_y + 1) \times (Z - N_z + 1)$ such blocks. We aim at matching each block in $\{\mathrm{B}\}$ with the block in $\{\mathrm{B}'\}$ maximizing a given similarity measure, which yields a "displacement field" between I and $S_K(I)$. Practically, it is not computationally feasible to make an exhaustive search of matchings within $\{\mathrm{B}'\}$ for each block of $\{\mathrm{B}\}$. In addition, we have an *a priori* knowledge about the position of the correspondent B' of B:

if the head is not too tilted, B′ is to be located in a neighborhood of B. Thus we constrain the search procedure to subsets defined as follows:

- We limit the search for correspondences to one block B every Δ_x (resp. Δ_y, Δ_z) voxels in the x (resp. y, z) direction, defining a subset of {B}; $\Delta = (\Delta_x, \Delta_y, \Delta_z)$ determines the density of the computed "displacement field" between I and $S_K(I)$.
- For each block B in this subset, we define a sub-image in $S_K(I)$, centered on B, which delimits a neighborhood of research. This sub-image is composed of the voxels in $S_K(I)$ located within a distance of Ω_x (resp. Ω_y, Ω_z) voxels in the x (resp. y, z) direction from B. This yields a rectangular parallelepipedic sub-image of size $(N_x + 2\Omega_x) \times (N_y + 2\Omega_y) \times (N_z + 2\Omega_z)$ in $S_K(I)$, which contains $(2\Omega_x+1)\times(2\Omega_y+1)\times(2\Omega_z+1)$ blocks B′ (provided this sub-image is entirely located in $S_K(I)$).
- In this sub-image, we examine one block B′ every Σ_x (resp. Σ_y, Σ_z) voxels in the x (resp. y, z) direction; $\Sigma = (\Sigma_x, \Sigma_y, \Sigma_z)$ determines the resolution of the displacement field.

Note that the subset of {B} in I and the subset of {B′} in the sub-image of $S_K(I)$ contain the following number of blocks, respectively:

$$\begin{array}{l} \max\{n_x | (n_x-1)\Delta_x + N_x \leq X\} \\ \times \max\{n_y | (n_y-1)\Delta_y + N_y \leq Y\} \\ \times \max\{n_z | (n_z-1)\Delta_z + N_z \leq Z\} \end{array} \quad \text{and} \quad \begin{array}{l} \max\{n_x | (n_x-1)\Sigma_x \leq 2\Omega_x\} \\ \times \max\{n_y | (n_y-1)\Sigma_y \leq 2\Omega_y\} \\ \times \max\{n_z | (n_z-1)\Sigma_z \leq 2\Omega_z\} \end{array}$$

We note B_{ijk} (resp. B'_{lnm}) the block in I (resp. $S_K(I)$) containing the voxel (i, j, k) (resp. (l, n, m)) at its top left back corner. We summarize the features of the algorithm as follows:

- For $(i = 0; i \leq X - N_x; i = i + \Delta_x)$
- For $(j = 0; j \leq Y - N_y; j = j + \Delta_y)$
- For $(k = 0; k \leq Z - N_z; k = k + \Delta_z)$
- We consider the block B_{ijk} in I
  - For $(l = i - \Omega_x; l \leq i + \Omega_x; l = l + \Sigma_x)$
  - For $(m = j - \Omega_y; m \leq j + \Omega_y; m = m + \Sigma_y)$
  - For $(n = k - \Omega_z; n \leq k + \Omega_z; n = n + \Sigma_z)$
  - If the block B'_{lnm} in $S_K(I)$ is entirely located in the image lattice, we compute a similarity measure with B_{ijk}
- We retain the block B'_{lnm} with maximal similarity measure, which defines the displacement vector between the center $(i + N_x/2, j + N_y/2, k + N_z/2)$ of B_{ijk} and the center $(l + N_x/2, n + N_y/2, m + N_z/2)$ of B'_{lnm}.

A given choice of parameters $N = (N_x, N_y, N_z)$, $\Omega = (\Omega_x, \Omega_y, \Omega_z)$, $\Delta = (\Delta_x, \Delta_y, \Delta_z)$, $\Sigma = (\Sigma_x, \Sigma_y, \Sigma_z)$, whose interpretation will be given later, yields pairs of correspondences (a_i, b'_i) between I and $S_K(I)$, a_i and b'_i being the centers of matched blocks. The output of this scheme is a displacement field, which conveys local information about brain symmetry or asymmetry. The points $\{b'_i\}$

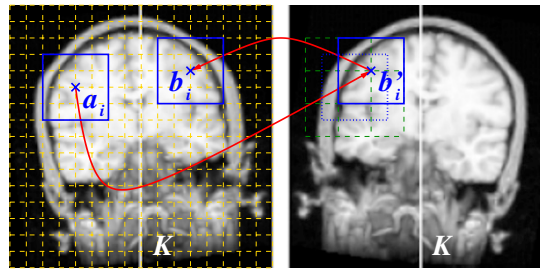

Fig. 4. The block matching. The point b'_i in $S_K(I)$ is homologous to the point a_i in I; $b_i = S_K(b'_i)$ is the counterpart of a_i in the other hemisphere. I contains 128^3 voxels. The chosen parameters are: $N = (32, 32, 32)$, $\Delta = (8, 8, 8)$, $\Omega = (8, 8, 8)$, $\Sigma = (16, 16, 16)$. In I, the subset of $\{\mathrm{B}\}$ is defined by the dashed grid (parameters Δ). Around the block of center a_i, superposed on $S_K(I)$ with dotted lines, a neighborhood of research is delimited (parameters Ω). In this sub-image of $S_K(I)$, the search is completed on the subset of $\{\mathrm{B}'\}$ defined by the small dashed grid (parameters Σ). For each of the $13^3 = 2197$ such defined blocks in I, the search is done on $2^3 = 8$ blocks in $S_K(I)$.

are then flipped back with respect to K, giving the points $\{b_i = S_K(b'_i)\}$; b_i is the counterpart of a_i in the opposite side of the brain (see Fig. 4).

Different intensity-based criteria can be chosen as a similarity measure, such as the Correlation Coefficient (CC) [2], the Correlation Ratio (CR) [14] or the Mutual Information (MI) [21,9]. Each of these measures assumes an underlying relationship between the voxel intensities of the 2 images, respectively affine (CC), functional (CR), or statistical (MI) [13]. Practically, the CR and the MI are well suited to multimodal registration, whereas the CC is suited to monomodal registration. In our case, I and $S_K(I)$ have the same "modality": an affine, or locally affine relationship can be assumed, and we use the CC.

This block matching approach, based on local similarity measures, allows to exclude very asymmetrical and meaningless areas from the computation of the plane. First, if no block B' in the subset defined in $S_K(I)$ exhibits a high —CC— with a given block B in the subset defined in I, its center is eliminated straightforwardly, by setting a convenient threshold. In practice, this happens when the structures existing in one given block in I are absent from any block in $S_K(I)$, which is the case for strongly asymmetrical areas. This elimination is not easily feasible in [12,19], where it is difficult to detect where the non-rigid algorithm fails. Thus, the estimation step, performed with these preselected interhemispheric correspondences, is mainly based on symmetrical areas. The robust estimation technique we use (a least trimmed squares minimization) allows to exclude the remaining asymmetrical areas from the computation of the plane.

Robust estimation of the mid-sagittal plane. A least trimmed squares (LTS) strategy is used to find the plane P best superposing the points $\{a_i\}$ and their counterparts $\{b_i\}$. This minimization scheme has been proven to be far more

robust to outliers than the classical LS method [15]. In our problem, we have to deal with two kinds of outlying measures. First, aberrant matchings can be obtained if the head is strongly tilted. Second, even after the initial short-listing that eliminates blocks with low —CC—, blocks conveying strong asymmetries can remain. This happens when a structure is present in both hemispheres, but in different locations: the two matched blocks containing this structure are likely to exhibit a high —CC—. The use of a robust estimation technique enables the computed plane to be only based on the underlying gross symmetry of the brain, the asymmetries being treated as outliers. The LTS scheme we use is:

- The plane P minimizing $\sum_i ||a_i - S_P(b_i)||^2$ is computed (see Appendix).
- The residuals $r_i = ||a_i - S_P(b_i)||$ are trimmed, and P is recomputed as previously, using only the voxels i with the 50% smaller residuals.
- After several iterations, the scheme stops when the angle between the normal vectors of two successively estimated planes is lower than a fixed threshold; we consider that they are "sufficiently close" to each other.

This strategy is able to cope with up to 50% of outliers [15]. To improve the accuracy of the estimation, we iterate the process (Fig. 5). As previously noted, after a first estimation P_1 of the mid-sagittal plane, the transformation $R_1 = (S_K \circ S_{P_1})^{1/2}$ is such that $P_1 = K$ in $R(I)$ (we recall that K is fixed to the image grid). We make a new block matching between $R_1(I)$ and $S_K(R_1(I))$, K being the firstly estimated plane P_1, and a new estimation P_2 by the LTS procedure. The transformation $R_2 = (S_K \circ S_{P_2})^{1/2}$ is such that $P_2 = K$ in $R_2 \circ R_1(I)$). After several iterations, the mid-sagittal plane P_n is computed from the image $(R_{n-1} \circ ... \circ R_1)(I)$. The final estimate is the plane K in $(R_n \circ ... \circ R_1)(I)$. The composition of the successively estimated rigid transformations R_i avoids multiple resampling. Usually, we choose a fixed number of iterations.

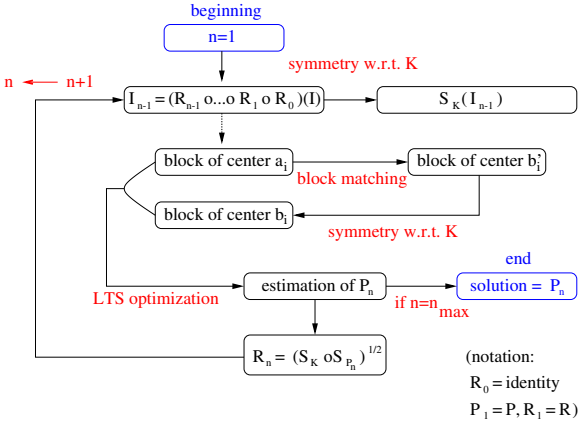

Fig. 5. General scheme. We describe the iterative process for one given choice of parameters (i.e., at one given scale). Usually, we fix the number of iterations: typically, $n_{max} = 5$ yields good results (see Section 3).

Multiscale scheme. Given a set of parameters N, Ω, Δ, Σ, the complexity of the block matching process is proportional to $\frac{(N_x N_y N_z)(\Omega_x \Omega_y \Omega_z)}{(\Delta_x \Delta_y \Delta_z)(\Sigma_x \Sigma_y \Sigma_z)}$ [11]. Intuitively, when I is strongly tilted, I and $S_K(I)$ are far from each other, and the neighborhood of research must be large (parameters Σ), to deal with strong differences in translation and rotation. We also expect large blocks (parameters N) to give more sensible CC than small ones. On the contrary, when I is already well aligned, we can restrict the neighborhood of research, and have more confidence in the CC computed on small blocks.

We implemented a multiscale scheme to achieve a good trade-off between accuracy and complexity. Initially, when the head is suspected to be strongly tilted, we make a first estimation of the mid-sagittal plane with large values of N, Ω, Δ, Σ. This raw estimate P_n^1, based on a displacement field with low density and low resolution, is the center of $(R_n^1 \circ ... \circ R^1)(I)$ (n is the number of iterations at a given scale). Then, we decrease the parameters so that the complexity remains constant: the new estimate P_n^2 is the center of $(R_n^2 \circ ... \circ R^2 \circ R_n^1 \circ ... \circ R^1)(I)$, and so on. At the last scale, the estimation is based on a displacement field of high density and high resolution, and is likely to be accurate. Usually, we make the following choices, for isotropic as well as anisotropic images:

- The initial values of the parameters are:
  - $N = ([X/4], [Y/4], [Z/4])$ or $N = ([X/8], [Y/8], [Z/8])$ (see Section 3)
  - $\Omega = N$, $\Delta = \Sigma = N/4$
- At each iteration, they are automatically updated as follows: $N \leftarrow N/2$, $\Omega \leftarrow \Omega/2$, $\Delta \leftarrow \Delta/2$, $\Sigma \leftarrow \Sigma/2$.
- The updating in the direction x (resp. y, z) stops when N_x (resp. N_y, N_z) is smaller than 4 at the next scale. At this level, the small block size makes the computed CC become meaningless. The whole process stops when there is no updating in any direction. For an image of size 128^3 and for each of the 2 choices we usually make for initial parameters, we get 4 and 3 scales respectively, and $\Delta = \Sigma = (1, 1, 1)$ at the last scale: this means that we obtain a displacement field of very high density and resolution.

3 Validation: Robustness and Accuracy Analysis

3.1 Materials

In this section, we present a series of experiments on simulated data, to show the robustness and the accuracy of the algorithm. Moreover, we aim at finding a set of optimal parameters for the computation of the plane and showing that the algorithm is robust with respect to a relatively high level of noise and bias. This simulated dataset contains 1152 synthetic MR images, generated as follows.

First, a perfectly symmetrical image I_1 is created. We consider an original MR image I of size 256^3, with voxel size 0.78mm^3, provided by Dr. Neil Roberts, Magnetic Resonance and Image Analysis Research Centre (University of Liverpool, UK). Running our algorithm on very high resolution images implies a

prohibitive computation time; we resample I to get a new image of size 128^3. In this latter, a mid-sagittal plane is determined by visual inspection, and matched with the center of the image grid. One half of the brain is removed; the other one is flipped with respect to the center, perfect symmetry plane of this new image I_1, which constitutes the ground truth for our validation experiments.

Second, artificial lesions with different grey levels and local expansions and shrinkings are added inside the brain to create strong focal asymmetries. Third, an additive, stationary, Gaussian white noise ($\sigma = 3$) is added, on top of the intrinsic noise in I_1. Fourth, a roll, a yaw angle and a translation along the left-right axis are applied. We choose the angles in the set {0, 3, 6,..., 21} (in degrees), and the translations in the set {0, 4, 8,..., 20} (in voxels): the 384 possible combinations constitute the dataset **A**; the applied noise is different for each image. Resampling I_1 to the size 64^3 gives the image I_2. Adding the same lesions and deformations, random noise with the same characteristics, and applying the same rotations, and translations of 0, 2,..., 10 voxels, we get a second dataset (**B**) of 384 images (the transformation with parameters (yaw,roll,translation)=$(\alpha, \beta, 2t)$ applied to I_1 and (α, β, t) applied to I_2 are the same). At last, a strong multiplicative bias field (linear in x, y and z) is added to I_2 before applying the transformation, which creates a third dataset (**C**) of 384 images. In brief:

- dataset A: I_1 + lesions + deformations + noise + 2 rotations + 1 translation
- dataset B: I_2 + lesions + deformations + noise + 2 rotations + 1 translation
- dataset C: I_2 + lesions + deformations + noise + bias + 2 rotations + 1 translation

3.2 Methods

The following experiments are devised (with $n_{max} = 5$ iterations at each scale):

- Experiment 1: dataset A with $(N, \Omega, \Delta, \Sigma) = (32, 32, 8, 8)$
- Experiment 2: dataset A with $(N, \Omega, \Delta, \Sigma) = (16, 16, 4, 4)$
- Experiment 3: dataset B with $(N, \Omega, \Delta, \Sigma) = (16, 16, 4, 4)$
- Experiment 4: dataset C with $(N, \Omega, \Delta, \Sigma) = (16, 16, 4, 4)$

For each experiment, the computed roll, yaw angles and translation along the left-right axis aligning the estimated mid-sagittal plane are compared with the applied ones, giving a measure of **accuracy** of the algorithm. For this purpose, the computed rigid transformation is composed with the applied one. The norm of the yaw and roll angles of the rotation component of this composition and the norm of its translation component along the left-right axis are computed; the closer to zero these 3 parameters are, the more accurate the result is. Another measure of accuracy ϵ is described in Fig. 7. We consider that an experiment is successful when ϵ is lower than a given threshold, typically, 1 voxel. The maximal value δ_{max} of δ (which measures the initial tilt of the head) for which the algorithm succeeds gives an idea of the **robustness** of the algorithm.

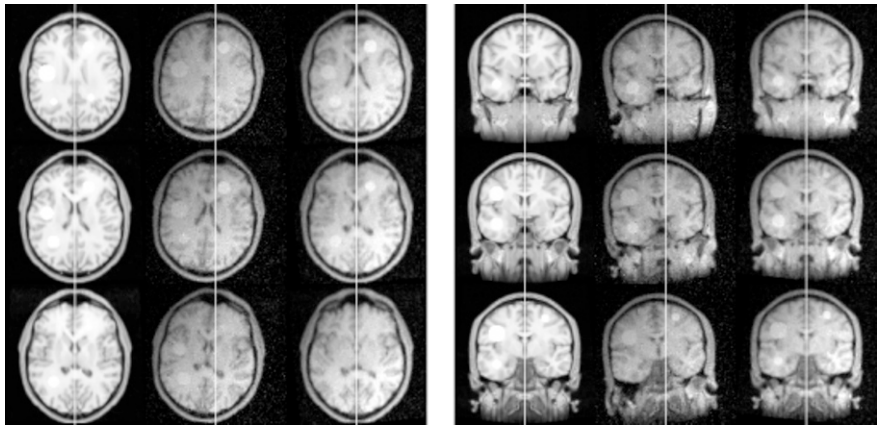

Fig. 6. Realignment of a synthetic MR image. Artificial lesions, local deformations, noise and bias are added to a perfectly symmetrical MR image of size 128^3. Roll and yaw angles of 6 degrees, and translation along the left-right axis of 6 voxels are applied to this image. The initial parameters of the block matching algorithm are $(N, \Omega, \Delta, \Sigma) = (16, 16, 4, 4)$. The errors of the computed transform, compared to the applied one are: 4.10^{-2} degrees (roll angle), 3.10^{-2} degrees (yaw angle), 10^{-1} voxels (translation), and 2.10^{-1} voxels (error ϵ, see Fig. 7). We display 2 panels with axial (left) and coronal (right) views. In each panel, from left to right, we have the original image with added lesions and deformations, the tilted image with added noise and bias, and the realigned and recentered image.

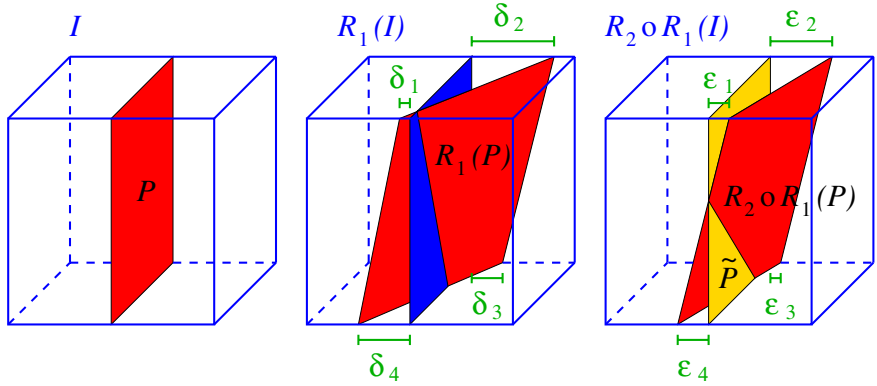

Fig. 7. A measure of accuracy. A synthetic image I is generated, in which the central plane P is the sought symmetry plane of the brain, as described in the text (left sketch). We apply yaw, roll angles, and a translation along the left-right axis, which yields a rigid transformation R_1. In $R_1(I)$, the real symmetry plane $R_1(P)$ is no longer aligned with the center of the image grid (central sketch). The maximum δ of the four distances $\delta_1, \delta_2, \delta_3, \delta_4$ measures the tilt of the head in $R_1(I)$ before we run the algorithm. We estimate a symmetry plane $\tilde{P}$ and a rigid transformation R_2 so that $\tilde{P}$ is displayed in the center of $R_2 \circ R_1(I)$ (right sketch). The estimated plane $\tilde{P}$ is generally different from the real one $R_2 \circ R_1(P)$. The maximum ϵ of the four distances $\epsilon_1, \epsilon_2, \epsilon_3, \epsilon_4$ gives a good idea of the maximal error in the whole volume of the image.

Comparing the experiments 1 and 2 (resp. 1 and 3) shows the influence of the initial size of the blocks (resp. subsampling) on the accuracy, the robustness and the computation time of the algorithm. This aims at indicating which set of parameters is best adapted to real medical images. Comparing the experiments 3 and 4 shows the sensitivity of the algorithm to bias effects. The experiments were led on a standard PC (OS Linux), 450 MHz, 256 MBytes of RAM.

3.3 Results and Interpretation

Experiment 1 *vs* **2.** The algorithm proved to be highly robust for the experiment 1. It never failed when δ was lower than 51 voxels, which corresponds (for example) to parameters (yaw,roll,translation)=$(15, 15, 16)$, $(18, 18, 8)$ or $(21, 21, 0)$. In real images, the tilt of the head is usually smaller. We noticed that the convergence of the algorithm is the same for parameters (α, β, t) and (β, α, t): the yaw and roll angles play symmetric roles. Note that this convergence is not deterministic in our experiments, because the random noise is added separately on each image of the datasets. Thus, the algorithm did not fail systematically for more extreme parameters; for example, it succeeded for the parameters $(21, 21, 20)$. For the experiment 2, the rate of success is significantly reduced: it systematically succeeded when δ was lower than 42, which approximately corresponds to parameters $(12, 12, 16)$, $(15, 15, 18)$ or $(18, 18, 0)$. The small initial block size and the restricted neighborhood of research explain that the algorithm is unable to deal with too tilted heads. Compared to experiment 1, there is one less scale to explore, and the average computation time is reduced, but still prohibitive (about 34 min). The obtained accuracy is about the same compared to experiment 1. Thus, the set of initial parameters $N = ([X/4], [Y/4], [Z/4])$ seems to be best adapted at a given resolution of the image.

Experiment 1 *vs* **3.** For these two datasets, studied with optimal initial block size, the robustness is about the same, surprisingly. The subsampling does not reduce significantly the efficiency of the algorithm, which can fail when δ is superior to 25 voxels, which corresponds to parameters $(15, 15, 8)$, $(18, 18, 4)$ or $(21, 21, 0)$, comparable with the parameters of experiment 1. The accuracy is divided by two in experiment 3 compared to experiments 1 and 2, but remains very high (see Table 1). At last, the computation time is strongly reduced (by a factor of 10). This suggests that highly subsampled images (from 256^3 to 64^3) are enough for a satisfying reorientation and recentering.

Experiment 3 *vs* **4.** The algorithm is very robust with respect to a relatively high bias. This is an important feature of this local approach. Locally, the intensity variations are smaller than on the whole image, and the CC is still a sensible measure. The accuracy and the computation time are similar.

Conclusion. We draw several conclusions from these experiments: the accuracy is always very high when the algorithm succeeds. For a usual MR image of size

256^3, with voxel size 0.78mm^3 and with an initial tilt of δ lower than about 100 voxels, which corresponds to realistic conditions of $\delta = 50$ (resp. 25) voxels in the subsampled image of size 128^3 (resp. 64^3), our algorithm is likely to succeed. Using the subsampled image of size 64^3, with $(16, 16, 4, 4)$ as initial parameters and 5 iterations at each scale, we reach a precision of about $\epsilon = 10.10^{-2} \times 4 \times 0.78 \simeq 0.3$ mm (see Table 1 and Fig. 7) for successful experiments, within a CPU time of about 3 minutes. For strongly tilted images, an initial alignment along the principal axes of the brain can be a useful preprocessing.

Table 1. Validation on simulated data. The RMS errors (indicated for successful experiments only) are measured in degrees for the angles and voxels for the left-right translation and the value ϵ (see Fig. 7). The errors are doubled between experiments on 128^3 and 64^3 images, including for the translation and ϵ (the errors in voxels are about the same, and the errors in mm are doubled for half resolution images).

Exp.	Robustness	Accuracy (RMS errors)				CPU
	(δ_{max})	Roll Angle	Yaw Angle	Translation	ϵ	Time
1	51 voxels	4.10^{-2}	4.10^{-2}	5.10^{-2}	11.10^{-2}	$45'$
2	42 voxels	3.10^{-2}	4.10^{-2}	5.10^{-2}	10.10^{-2}	$34'$
3	25 voxels	11.10^{-2}	9.10^{-2}	6.10^{-2}	13.10^{-2}	3'
4	25 voxels	11.10^{-2}	8.10^{-2}	7.10^{-2}	11.10^{-2}	$3'$

4 Results and Acknowledgements

In this section, we present results for real anatomical (MR, CT) and functional (SPECT, PET) images. For each illustration, we present axial (top) and coronal (bottom) views, for the initial 3D image (left) and the reoriented and recentered version (right) (see Fig. 8). The MR image has been provided by Dr. Neil Roberts, Magnetic Resonance and Image Analysis Research Centre (University of Liverpool, UK), and is of size 256^3, with voxel size 0.78mm^3. The CT image comes from the Radiology Research Imaging Lab (Mallinckrodt Institute of Radiology, Saint Louis, Missouri, USA), and is of size $256 \times 256 \times 203$, with voxel size $0{,}6\text{mm}^3$. The SPECT image has been provided by Pr. Michael L. Goris, Department of Nuclear Medicine (Stanford University Hospital, USA), and is of size 64^3. At last, the PET image has been provided by the Hammersmith Hospital in London, UK, and the Unité 230 of INSERM, Toulouse, France. It is of size $128 \times 128 \times 15$, with voxel size 2.05mm $\times$ 2.05mm $\times$ 6.75mm.

5 Conclusion

We have presented a new symmetry-based method allowing to compute, reorient and recenter the mid-sagittal plane in volumetric anatomical and functional images of the brain. Our approach relies on the matching of homologous anatomical structures or functional areas in both sides of the brain (or the skull), and a

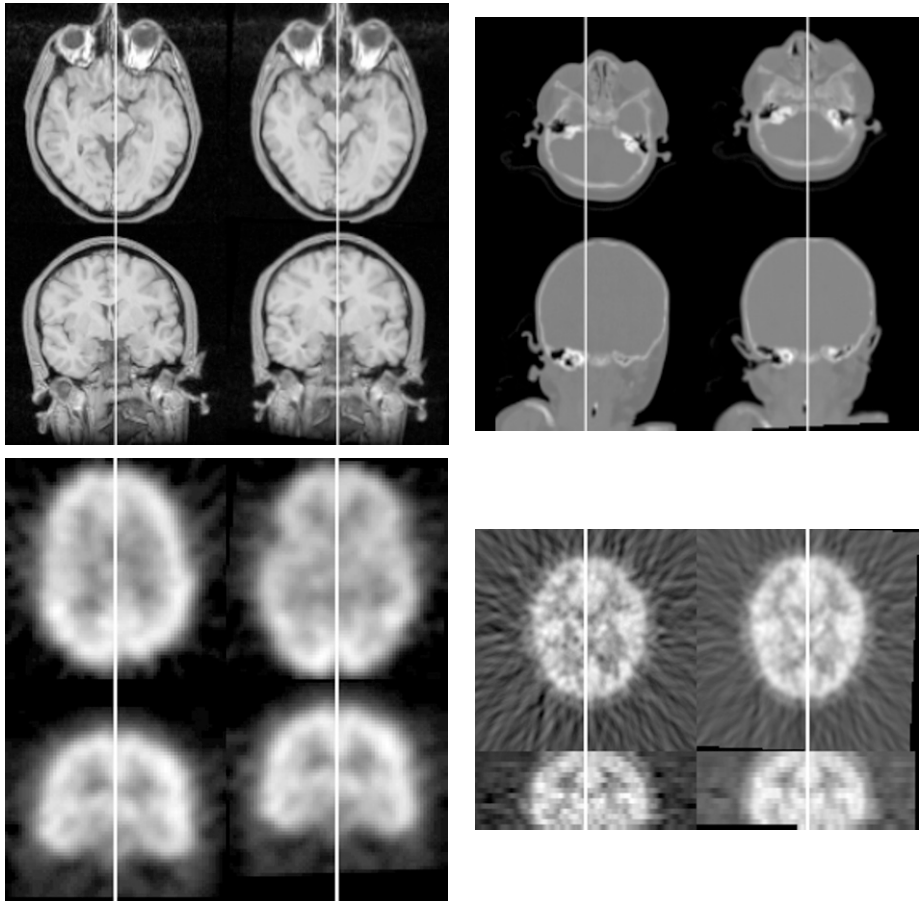

Fig. 8. Results on real images. From left to right, top to bottom: isotropic MR, CT, SPECT images, and anisotropic PET image. See Section 4 for details.

robust estimation of the plane best superposing these pairs of counterparts. The algorithm is iterative, multiscale, fully automated, and provides a useful tool for further symmetry-based analysis of the brain. We showed on a large database of synthetic images that we could obtain a subvoxel accuracy in a CPU time of about 3 minutes for strongly tilted heads, noisy and biased images. We have presented results on isotropic or anisotropic MR, CT, SPECT and PET images; the method will be tested on functional MR and ultrasound images in the future.

Appendix: LS Estimation of the Mid-Sagittal Plane

We want to minimize $C = \sum_i (S(b_i) - a_i)^2$, with $S(b_i) = b_i - 2((b_i - p)^\top n)n$ and where p is a point in the plane and n the unit normal vector to the plane. By differentiating C with respect to p, we get:

$$\frac{dC}{dp} = 4\sum_i (2p - b_i - a_i)^\top nn^\top$$

which demonstrates that the barycenter $G = \frac{1}{n}\sum_i \frac{(b_i+a_i)}{2}$ belongs to the plane. Substituting G in the first equation, we get:

$$C = \sum_i (b_i - a_i)^2 + 4[(b_i - G)^\top n][(a_i - G)^\top n]$$

which is minimized when the following expression is minimized:

$$\sum_i n^\top [(a_i - G)(b_i - G)^\top] n$$

which means than n is the eigenvector associated to the smallest eigenvalue of I, where:

$$I = \sum_i (a_i - G)(b_i - G)^\top$$

References

1. B.A. Ardenaki, J. Kershaw, M. Braun, and I. Kanno. Automatic Detection of the Mid-Sagittal Plane in 3-D Brain Images. *IEEE Transactions on Medical Imaging*, 16(6):947–952, December 1997.
2. L.G. Brown. A survey of image registration techniques. *ACM Computing Surveys*, 24(4):325–375, December 1992.
3. M.E. Brummer. Hough Transform Detection of the Longitudinal Fissure in Tomographic Head Images. *IEEE Transactions on Medical Imaging*, 10(1):74–81, March 1991.
4. T.J. Crow. Schizophrenia as an anomaly of cerebral asymmetry. In K. Maurer, editor, *Imaging of the Brain in Psychiatry and Related Fields*, pages 1–17. Springer-Verlag, Berlin Heidelberg, 1993.
5. N. Geschwind and W. Levitsky. Left-right asymmetry in temporal speech region. *Science*, 161:186–187, 1968.
6. R. Guillemaud, A. Marais, P. amd Zisserman, B. McDonald, and T.J. Crow. A 3-Dimensional Midsagittal Plane For Brain Asymmetry Measurement. *Schizophrenia Research*, 18(2-3):183–184, 1995.
7. L. Junck, J.G. Moen, G.D. Hutchins, M.B. Brown, and D.E. Kuhl. Correlation Methods for the Centering, Rotation, and Alignment of Functional Brain Images. *Journal of Nuclear Medicine*, 31:1220–1226, July 1990.
8. Y. Liu, R.T. Collins, and W.E. Rothfus. Automatic Bilateral Symmetry (Midsagittal) Plane Extraction from Pathological 3D Neuroradiological Images. In *SPIE, International Symposium on Medical Imaging*, San-Diego, CA, February 1998.
9. F. Maes, A. Collignon, Vandermeulen. D., G. Marchal, and P. Suetens. Multimodality Image Registration by Maximization of Mutual Information. *IEEE Transactions on Medical Imaging*, 16(2):187–198, April 1997.

10. S. Minoshima, K.L. Berger, K.S. Lee, and M.A. Mintun. An Automated Method for Rotational Correction and Centering of Three-Dimensional Functional Brain Images. *Journal of Nuclear Medicine*, 33:1579–1585, August 1992.
11. S. Ourselin, A. Roche, G. Subsol, and X. Pennec. Automatic Alignment of Histological Sections. In F. Pernuš, S. Kovačič, H.S. Stiehl, and M.A. Viergever, editors, *International Workshop on Biomedical Image Registration, WBIR'99*, pages 1–13, Bled, Slovenia, August 1999. Electronic version: http://www.inria.fr/RRRT/RR-3595.html.
12. S. Prima, J.-P. Thirion, G. Subsol, and N. Roberts. Automatic Analysis of Normal Brain Dissymmetry of Males and Females in MR Images. In W.M. Wells, A. Colchester, and S. Delp, editors, *First International Conference on Medical Image Computing and Computer-Assisted Intervention, MICCAI'98*, volume 1496 of *Lecture Notes in Computer Science*, pages 770–779, Boston, USA, October 1998. Springer.
13. A. Roche, G. Malandain, N. Ayache, and S. Prima. Towards a Better Comprehension of Similarity Measures Used in Medical Image Registration. In C. Taylor and A. Colchester, editors, *Second International Conference on Medical Image Computing and Computer-Assisted Intervention, MICCAI'99*, volume 1679 of *Lecture Notes in Computer Science*, pages 555–566, Cambridge, UK, September 1999. Springer. Electronic version: http://www.inria.fr/RRRT/RR-3741.html.
14. A. Roche, G. Malandain, X. Pennec, and N. Ayache. The Correlation Ratio as a New Similarity Measure for Multimodal Image Registration. In W.M. Wells, A. Colchester, and S. Delp, editors, *First International Conference on Medical Image Computing and Computer-Assisted Intervention, MICCAI'98*, volume 1496 of *Lecture Notes in Computer Science*, pages 1115–1124, Boston, USA, October 1998. Springer. Electronic version: http://www.inria.fr/RRRT/RR-3378.html.
15. P.J. Rousseuw and A.M. Leroy. *Robust Regression and Outlier Detection.* Wiley Series In Probability And Mathematical Statistics, 1987.
16. S. Smith and M. Jenkinson. Accurate Robust Symmetry Estimation. In C. Taylor and A. Colchester, editors, *Second International Conference on Medical Image Computing and Computer-Assisted Intervention, MICCAI'99*, volume 1679 of *Lecture Notes in Computer Science*, pages 308–317, Cambridge, UK, September 1999. Springer.
17. C. Sun and J. Sherrah. 3D Symmetry Detection Using The Extended Gaussian Image. *IEEE Transactions on Pattern Analysis and Machine Intelligence*, 19(2):164–168, 1997.
18. J.-P. Thirion. Image matching as a diffusion process: an analogy with Maxwell's demons. *Medical Image Analysis (MedIA)*, 2(3):243–260, September 1998.
19. J.-P. Thirion, S. Prima, G. Subsol, and N. Roberts. Statistical Analysis of Normal and Abnormal Dissymmetry in Volumetric Medical Images. *Medical Image Analysis (MedIA)*, 4(2), 2000. Electronic version: http://www.inria.fr/RRRT/RR-3178.html.
20. A. Venot, J.F. Lebruchec, and J.C. Roucayrol. A New Class of Similarity Measures for Robust Image Registration. *Computer Vision, Graphics, and Image Processing*, 28(2):176–184, 1984.
21. W.M. Wells III, P. Viola, H. Atsumi, S. Nakajima, and R. Kikinis. Multi-modal volume registration by maximization of mutual information. In *Medical Image Analysis*, volume 1, pages 35–51. Oxford University Press, March 1996.
22. T.H. Williams, N. Gluhbegovic, and J.Y. Jew. Virtual Hospital. 1997. University of Iowa. WEB access: http://www.vh.org/Providers/Textbooks/BrainAnatomy/-BrainAnatomy.html.